Published in final edited form as:

Structure. 2020 August 04; 28(8): 910–921.e4. doi:10.1016/j.str.2020.04.023.

Structural and functional analyses of the FAM46C/Plk4 complex

Hua Chen[1,3], **Defen Lu**[1,3], **Guijun Shang**[1], **Guoming Gao**[1], **Xuewu Zhang**[1,2,4]

[1]Department of Pharmacology, University of Texas Southwestern Medical center, Dallas, Texas, USA, 75390

[2]Department of Biophysics, University of Texas Southwestern Medical center, Dallas, Texas, USA, 75390

Summary

FAM46C, a non-canonical poly(A) polymerase, is frequently mutated in multiple myeloma. Loss-of-function of FAM46C promotes cell survival of multiple myeloma, suggesting a tumor-suppressive role. FAM46C is also essential for fastening sperm head and flagellum, indispensable for male fertility. The molecular mechanisms of these functions of FAM46C remain elusive. We report the crystal structure of FAM46C to provide the basis for its poly(A) polymerase activity and rationalize mutations associated with multiple myeloma. In addition, we found that FAM46C interacts directly with the serine/threonine kinase Plk4, the master regulator of centrosome duplication. We present the structure of FAM46C in complex with the Cryptic Polo-Box 1–2 domains of Plk4. Our structure-based mutational analyses show that the interaction with Plk4 recruits FAM46C to centrosomes. Our data suggest that Plk4-mediated localization of FAM46C enables its regulation of centrosome structure and functions, which may underlie the roles for FAM46C in cell proliferation and sperm development.

Blurb:

FAM46C, a non-canonical poly-A polymerase, is important for sperm development and tumor suppression. Here Chen, Lu et al identify a direct interaction between FAM46C and Plk4 in the centrosome, suggesting a pathway that may underlie the functions of FAM46C. The crystal structures of FAM46C and the FAM46C/Plk4 complex are presented.

Graphical Abstract

[4]Corresponding author and lead contact: Xuewu.zhang@utsouthwestern.edu.

Author contributions. G.S., H.C. and X.Z. conceived the project. G.S., H.C., G.G. and X.Z. determined the crystal structures. H.C., G.S. and G.G. carried out the biochemical analyses. D.L. and H.C. performed the cell-based experiments. H.C., D.L., G.S. and X.Z. wrote the manuscript.

[3]These authors contributed equally

Declaration of Interests. The authors declare no competing interests.

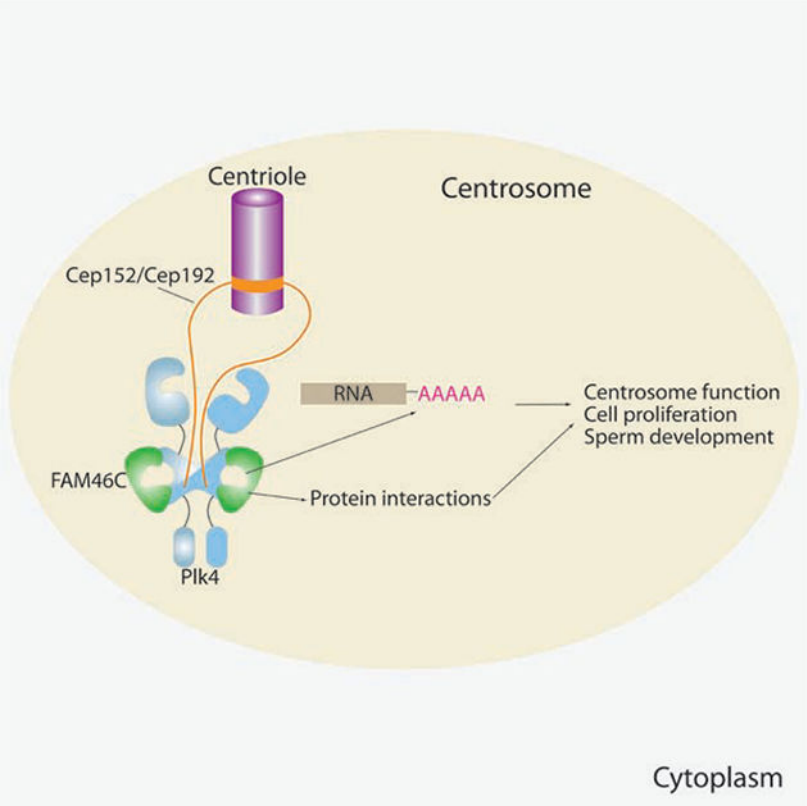

Introduction

Family with sequence similarity 46 (FAM46) are proteins evolutionarily conserved from ameobozoa to vertebrates, with important but poorly understood biological functions (Kuchta et al., 2016). The human proteome contains four FAM46 family members: FAM46A, B, C and D. Mutations of the *FAM46* genes have been implicated in human diseases (Kuchta et al., 2016). For example, mutations of *FAM46A* are linked to non-small cell lung cancer, bone abnormalities and familial autosomal recessive retinitis pigmentosa (Barragan et al., 2008; Diener et al., 2016; Etokebe et al., 2015). FAM46B has been shown to play regulatory roles in embryonic stem cells (Hu et al., 2020). Strikingly, a number of recent studies have found that *FAM46C* is one of the most frequently mutated genes in multiple myeloma (Barbieri et al., 2016; Bolli et al., 2014; Boyd et al., 2011; Chapman et al., 2011; Walker et al., 2015; Walker et al., 2012; Zhu et al., 2015). These studies show that *FAM46C* mutations are found in over 20% patients and associated with poor survival prognosis. Many of these are loss-of-function mutations such as homozygous deletions or frameshift insertions, suggesting that FAM46C is a tumor suppressor. Consistently, ectopic expression of wild type FAM46C has been shown to inhibit proliferation and promote apoptosis of myeloma and other cell types (Mroczek et al., 2017; Zhang et al., 2017; Zhu et al., 2017). In addition, a recent study has shown that FAM46C is localized in the manchette of mouse spermatids, a transient microtubule-based platform in the perinuclear region that is involved in re-shaping spermatid head and protein transport (Zheng et al., 2019). Consistent with this localization, genetic knockout of *FAM46C* in mice leads to male sterility because

these mice only produce headless spermatozoa (Zheng et al., 2019). The molecular basis for these functions of FAM46C are largely unknown.

The FAM46 proteins all contain a conserved domain of ~330 residues that is flanked by short variable N- and C-terminal extensions (Figure 1A). The conserved domain shows sequence similarity to nucleotidyltransferases (NTase), which catalyze the transfer of nucleoside monophosphate (NMP) from nucleoside triphosphate (NTP) to an acceptor hydroxyl group on nucleic acids, proteins or small molecules (Kuchta et al., 2009; Kuchta et al., 2016). Recent studies have confirmed that the FAM46 proteins are indeed NTases, specifically, non-canonical poly(A) polymerases that add a stretch of AMP derived from ATP to the 3'-end of RNA (Hu et al., 2020; Mroczek et al., 2017). It has been shown that FAM46C increases expression of many genes in cells in a manner dependent on its poly(A) polymerase activity, which likely acts through polyadenylating RNA targets and thereby enhancing their stability (Mroczek et al., 2017). It has been suggested that FAM46C controls antibody production through polyadenylation of immunoglobulin mRNAs (Herrero et al., 2020). The cytotoxic and cytostatic effects of FAM46C on multiple myeloma is also dependent on the poly(A) polymerase activity (Mroczek et al., 2017). Other non-canonical poly(A) polymerases do not have such cytotoxic affects, suggesting that FAM46C uses a unique mechanism to control cell proliferation and survival of multiple myeloma. This mechanism remains unclear, as many genes are regulated but no specific ones have been found to be responsible for the inhibitory effect of FAM46C on cell proliferation. On the other hand, the function of FAM46C in spermatids does not seem to rely on its global regulation of mRNA, as FAM46C knockout only significantly alters the mRNA levels of a few genes in testes (Zheng et al., 2019).

To pinpoint the molecular pathways in which the FAM46 proteins function, we sought to identify their binding partners in cells. The BioGRID database annotates a potential interaction between FAM46C and the serine/threonine kinase Polo-like kinase 4 (Plk4) based on a large-scale yeast two-hybrid screen (Rual et al., 2005; Stark et al., 2006). Here we show that FAM46C interacts directly with Plk4 both in cells and in vitro. Plk4 is the master regulator of centrosome duplication, which occurs once per cell cycle to instruct the formation of the bi-polar mitotic spindle for proper segregation of chromosomes to daughter cells (Bettencourt-Dias et al., 2005; Habedanck et al., 2005). The protein level and kinase activity of Plk4 are tightly regulated in normal cells (Cunha-Ferreira et al., 2013; Holland et al., 2012; Holland et al., 2010; Klebba et al., 2015; Lopes et al., 2015; Sillibourne et al., 2010). Overexpression of Plk4 promotes centrosome overduplication, leading to aneuploidity and in some cases tumorigenesis depending on the genetic background (Coelho et al., 2015; Levine et al., 2017; Sercin et al., 2016; Vitre et al., 2015). There is evidence suggesting the association of centrosome overduplication and multiple myeloma (Dementyeva et al., 2010). Small molecule inhibitors of Plk4 have been developed for cancer therapy (Mason et al., 2014; Wong et al., 2015). The finding of the direct interaction between FAM46C and Plk4 suggests a functional role for FAM46C in the centrosome, which may underlie its tumor suppressor activity in multiple myeloma. The Plk4-mediated localization of FAM46C to the centrosome also provides a link to the role of FAM46C in the spermatid manchette, which has been suggested to be nucleated by the centrosome (Lehti and Sironen, 2016).

In addition to the kinase domain, Plk4 contains two Cryptic Polo-Box domains (CPB1 and CPB2) and one Polo-Box domain (PB3) (Figure 1A). CPB1 and CPB2 together form an integrated X-shaped dimeric module (Park et al., 2014; Shimanovskaya et al., 2014; Slevin et al., 2012). Two proteins in the pericentriolar material (PCM), centrosomal protein 192 (Cep192) and 152 (Cep152), bind CPB1–2 of Plk4 and recruit it to the mother centriole to initiate the duplication process (Kim et al., 2013; Park et al., 2014). PB3 in Plk4 binds SAS5/STIL/Ana2, another key regulator in centrosome duplication (Arquint et al., 2015; Leung et al., 2002; Moyer et al., 2015; Ohta et al., 2014). We found that CPB1–2 in Plk4 is necessary and sufficient for the interaction with FAM46C. We solved the crystal structures of the FAM46C/CPB1–2 binary complex and the FAM46C/CPB1–2/CEP192 ternary complex. We further showed that the inhibition of cell proliferation by FAM46C is dependent on its interaction with Plk4. Our data support a model that Plk4 recruits FAM46C into the centrosome, which may contribute to the functions of FAM46C in the regulation of cell cycle and spermatid development.

Results

Direct interaction between CPB1–2 of Plk4 and the FAM46 family proteins.

To investigate the potential interaction between FAM46C and Plk4 as indicated by the previous high-throughput yeast two-hybrid study (Rual et al., 2005), we co-expressed the two proteins in HEK293 cells. Co-immunoprecipitation experiments showed that FAM46C was able to pull-down the full-length Plk4 (Figure 1B). Two constructs of Plk4 containing both CPB1–2 and PB3 (residues 580–810 and 580–970, respectively) also bound to FAM46C, whereas the kinase domain of Plk4 (residues 1–272) did not. To verify that the interaction is direct, we carried out pull-down assays with purified recombinant proteins. GST-tagged FAM46C pulled-down CPB1–2 but not PB3 of Plk4 (Figure 1C). The pull-down assay showed that FAM46D also interacts with CPB1–2 of Plk4 (Figure 1D). These results together suggest that the interaction with CPB1–2 of Plk4 is a conserved function of the FAM46 family proteins.

We then carried out poly(A) elongation assays using fluorescein-labelled RNA oligos as primers to examine whether the interaction with CPB1–2 of Plk4 affects the poly(A) polymerase activity of FAM46. We used FAM46D for the enzymatic assays throughout the study because it has been shown that the poly(A) polymerase activity of FAM46D is much higher than that of other FAM46 family members and therefore easier to detect (Mroczek et al., 2017). The presence of CPB1–2 did not change the length of the poly(A) products catalyzed by FAM46D (Figure 1E), suggesting that CPB1–2 binding does not regulate the poly(A) polymerase activity. We also tested whether FAM46D could be phosphorylated by Plk4. The results from a Phos-tag gel assay showed that while the kinase domain of Plk4 phosphorylated itself as well as the generic serine/threonine-kinase substrate myelin basic protein (MBP), it did not phosphorylate the NTase domain of FAM46D (Figure 1F). These results suggest that it is unlikely that Plk4 regulates FAM46 by phosphorylating its enzymatic domain, although the possibility of phosphorylation of the FAM46 N- and C-terminal extensions by Plk4 cannot be excluded.

Crystal structure of FAM46C.

To understand the molecular basis of the poly(A) polymerase activity of FAM46C, we determined the crystal structure of the NTase domain of human FAM46C to 2.7 Å resolution (Table 1). FAM46C adopts an overall bi-lobal structure characteristic of NTase family enzymes (Figure 2A). The structure is very similar to the recently reported structure of FAM46B from *Xenopus tropicalis* (Hu et al., 2020) (Figure 2D), with the root mean square deviation (r.m.s.d) of 1.6 Å for the 304 aligned Cα atoms, despite the low level of sequence identity (24%) between the two proteins. The N- and C-terminal lobes are referred to as the catalytic and central domains, respectively (Figure 1A and 2A) (Martin and Keller, 2007). A search of the protein structural database with the DALI server showed that FAM46C are structurally similar to poly(A) polymerases and tRNA CCA-adding enzymes (Holm et al., 2008). However, FAM46C only contains the core NTase domain but not the RNA binding domain that is present in those canonical RNA polymerases, and therefore is categorized as a non-canonical poly(A) polymerase (Nakel et al., 2015). Moreover, the conformation of FAM46C is substantially different from canonical RNA polymerases, with the r.m.s.d. over 3 Å relative to all the hits identified by DALI.

The N-terminal catalytic domain of FAM46C is composed of a 7-stranded β-sheet that is covered by 6 α-helices on the top (Figure 2A). An amphipathic 3-turn helix spanning residues 219–228 connects the catalytic domain to the central domain, which is composed of a 5-helix bundle. The large cleft between these two domains forms the substrate-binding pocket. The cleft and its periphery contain many positively charged residues. As a result, the entrance of the cleft shows strong positive electrostatic potential, which likely plays a role in binding the RNA substrate (Figure 2B). Inside the cleft, the inner face of the catalytic domain contains the three conserved motifs that are important for catalysis, GS (Gly73-Ser74), [D/E]h[D/E]h (Asp90-Leu91-Asp92-Leu93) and h[D/E]h (Val165-Glu166-Leu167) (h: hydrophobic residue) (Figure 2A and Figure S1). According to the positions in the active site, Gly73/Ser74 and Asp90/Asp92 are responsible for binding nucleotide and magnesium ion respectively, while Glu166 acts as the catalytic residue (Martin and Keller, 2007). These motifs are conserved in all FAM46 family members and other NTases (Figure S1) (Kuchta et al., 2009; Kuchta et al., 2016). Mutations of Asp90 or Asp92 have been shown to abolish the poly(A) polymerase activity of FAM46C (Mroczek et al., 2017). We found that an E158Q mutation in FAM46D (equivalent to E166Q in FAM46C) also abolished the activity (See below).

A large number of mutations have been found throughout the coding region of the *FAM46C* gene in multiple myeloma (Barbieri et al., 2016). Insertions, deletions and non-sense mutations likely cause gross disruption of the structural integrity of the protein. To understand the effects of the mis-sense mutations, we mapped them to the crystal structure of FAM46C (Figure 2C), which suggests that many of the mutations perturb either the active site or the structure of FAM46C. For example, the mutations of Asp90 and Glu166, two of the key active site residues, are expected to abrogate the enzymatic activity of FAM46C. Many other mutations are targeted to residues in the hydrophobic core, resulting in destabilization of the protein. These analyses together provide a structural basis for understanding the cancer-associated mutations in FAM46C, supporting the notion that the

tumor suppressor role of FAM46C is dependent on both its structural integrity and poly(A) polymerase activity.

Crystal structure of the FAM46C/CPB1–2 and FAM46C/CPB1–2/CEP192 complexes.

To uncover how FAM46C and Plk4 interact, we determined the crystal structure of the complex between FAM46C and CPB1–2 from Plk4 at 4.5 Å resolution (Table 1). A previous structural study has shown that residues 214–242 in Cep192 bind CPB1–2 of Plk4 and thereby recruit Plk4 to the mother centriole to initiate the duplication (Park et al., 2014). We co-crystallized this segment of Cep192 with FAM46C and CPB1–2 and solved the structure of the ternary complex to 4.4 Å resolution. Based on these structures, we designed a $FAM46C^{E166Q/F193D/F206D}$ mutant and used it to obtain crystals of the $FAM46C^{E166Q/F193D/F206D}$/CPB1–2 complex in a different crystal form, which diffracted to 3.8 Å resolution (Figure 3A; See methods for details). The conformations of the individual proteins and the interactions between FAM46C and CPB1–2 are similar in the three structures, except that in the new crystal form the inter-domain angle between CPB1 and CPB2 is different to some extent (Figure S3 and S4). The following descriptions will refer to the higher resolution structure of the $FAM46C^{E166Q/F193D/F206D}$/CPB1–2 complex unless otherwise stated.

FAM46C adopts essentially the same conformation as in the apo-structure (Figure S3A). Likewise, CPB1–2 forms the X-shaped dimer as seen in the previously reported structures, with the β-sheets in CPB2 pack side-by-side to form an integrated, extended β-sheet (Figure S3B) (Park et al., 2014; Shimanovskaya et al., 2014). Therefore, the interaction does not induce substantial conformational changes to either FAM46C or CBP1–2. The two FAM46C molecules bind to the two opposite sides of the CPB1–2 dimer in a symmetric fashion. The previous structural analyses have shown that the positively charged top surface of the CPB1–2 dimer binds the negatively charged motifs from Cep192 and Cep152 (Park et al., 2014). The binding surface for Cep192 and Cep152 is unoccupied in the FAM46C/PB1–2 complex structure (Figure 3A). These observations suggest that CPB1–2 can simultaneously binding to both FAM46C and Cep192 or Cep152, which is confirmed by our structure of the ternary complex (Figure 3B). The binding mode of the Cep192 peptide in this structure is essentially the same as seen in the structure of the CPB1–2/Cep192 binary complex (Figure S4) (Park et al., 2014).

Details of the FAM46C/CBP1–2 binding interfaces and mutational analyses.

FAM46C engages the CPB1–2 dimer through two separate interfaces (Figure 4A). Interface I is formed by a side-by-side β-sheet packing interaction between the N-terminal catalytic domain of FAM46C and CPB1 from one protomer of the CPB1–2 dimer. The outer β-strand from FAM46C (residues 140–146) packs with its counterpart in CPB1 (residues 669–674) parallelly. While the low resolution of the structure prevents detailed analyses of the specific atomic interactions, this packing pattern suggests that the two β-strands interact through backbone hydrogen bonds as in regular β-sheets as well as van der Walls interactions. This interface combines the β-sheets in CPB1 and FAM46C into one expanded β-sheet, resembling the β-sheet integration that mediates the formation of the CPB1–2 dimer. As a consequence of the β-sheet interaction, the edge of CPB1 is placed near the opening of the

substrate binding cleft in FAM46C but does not obstruct it (Figure 4A), which explains the fact that the CPB1–2 of Plk4 does not affect the poly(A) polymerase activity (Figure 1E).

Interface II between FAMP46C and CPB1–2 is formed by a loop (residues 318–323) connecting two helices in the central domain of FAM46C and a pocket at the side of CPB2 from the second protomer in the CPB1–2 dimer (Figure 4A). Cys320 and Leu321 in the loop of FAM46C make hydrophobic interactions with Phe727, Tyr709, Met767 and Tyr768 in CPB2 that line the hydrophobic pocket. Interestingly, mutations of Cys320 have been found in multiple myeloma (Figure 2C), suggesting that this residue is functionally important (Barbieri et al., 2016). The residues of both interfaces I and II are conserved in the FAM46 family (Figure S1), consistent with our results that other members of the family also bind CPB1–2 of Plk4.

We designed mutations to test the binding mode between FAM46C and CPB1–2 shown by the crystal structure. The packing interactions mediated by the β-strands in interface I is likely dependent more on the secondary structure and shape complementarity than the sidechains of the residues. We therefore mutated a number of interface I residues in either FAM46C or CPB1–2 to proline to perturb the β-strands. The results of the pulldown binding assays show that proline mutations of either Lys144 or Cys146 in the middle of the interface β-strand of FAM46C decreased the FAM46C/CPB1–2 interaction substantially (Figure 4B). The results are similar with the I670P mutation of the interface β-strand of CPB1–2 (Figure 4C). The proline mutants expressed at similar or slightly reduced levels compared to the respective wild types, and ran as mono-disperse peaks on gel filtration columns. In addition, FAM46D containing a K136P mutation, equivalent to FAM46C(K144P), remains catalytically active (see below). These results together suggest that the observed effects of the proline mutations on the FAM46C/CPB1–2 interaction is due to disruption of the binding interface, rather than gross misfolding of the mutant proteins. As a comparison, the N669R mutation at the N-terminal end of the β-strand in CPB1–2 did not affect the binding (Figure 4C). We also tested the contribution of interface II to the interaction by mutating Cys320 and Leu321 in FAM46C. The results show that the C320E/L321E double mutations decreased the binding to CPB1–2 slightly (Figure 4B). Combining these double mutations with interface I mutations in FAM46C (K144P/C320E/L321E and C146P/C320E/L321E) led to much weakened binding to CPB1–2 (Figure 4B). These results together confirm the interfaces seen in the crystal structures are responsible for the FAM46C/CPB1–2 interaction.

FAM46C is recruited to centrosome by Plk4 but does not affect Plk4-mediated centrosome overduplication.

The fact that CPB1–2 of Plk4 can simultaneously bind FAM46C and Cep192 suggests that Plk4 may recruit FAM46C to centrosomes. To test this idea, we co-expressed FAM46C and Plk4 in U2OS cells and examined their localization using immuno-fluorescence microscopy. As expected, full-length wild type (WT) Plk4 mostly localized to a few strong dots in cells that coincide with the centrosome maker protein -tubulin (Figure 5A). It has been shown previously that ectopically expressed FAM46C is broadly distributed in both the cytosol and nucleus (Mroczek et al., 2017). Our results show that when co-expressed with Plk4 in these cells, a fraction of FAM46C formed bright puncta that colocalized with both Plk4 and -

tubulin in centrosomes (Figure 5A). We then tested the I670P mutant of Plk4, which does not bind to FAM46C (Figure 4C). Plk4(I670P) expressed in U2OS cells localized to centrosomes similar to Plk4(WT), but failed to recruit co-expressed FAM46C (Figure 5A). These results demonstrate that FAM46C can be recruited to centrosomes through its interaction with the CBP1–2 domain of Plk4 as seen in our crystal structures.

Next we examined whether FAM46C regulates Plk4-mediated centrosome overduplication. We established a U2OS cell line that contains the *Plk4* gene under the control of a doxycycline-inducible promoter (see methods for details). As expected, forty-eight hours after the induction of Plk4 expression, approximately 60% cells contained more than four centrioles (Figure 5B). Consistent with the results in Figure 5A, the FAM46C wild type or the catalytically dead mutant (E166Q) co-expressed with Plk4 in these cells co-localized well with Plk4 in centrosomes (Figure 5B). Co-expression of FAM46C however did not change the percentage of cells with more than four centrioles (Figure 5B), suggesting that FAM46C does not regulate Plk4-mediated centrosome overduplication.

Cell growth inhibition by FAM46C relies on its interaction with Plk4.

Previous studies have shown that expression of FAM46C in several multiple myeloma cell lines, which lack functional FAM46C due to loss-of-function mutations, causes reduced cell survival and increased apoptosis (Mroczek et al., 2017; Zhang et al., 2017; Zhu et al., 2017). The cytotoxic effect of FAM46C is abrogated by mutations of one of the catalytic motifs (D90A/D92A), suggesting that the poly(A) polymerase activity is important for this function of FAM46C (Mroczek et al., 2017). Using the same assay as in (Zhu et al., 2017), we confirmed that expression of wild type FAM46C for 6 days in the multiple myeloma cell line MM1.S reduced cell viability/proliferation by ~50% as compared with the parental cell line cultured under the same conditions (Figure 6A). As expected, FAM46C with the catalytic residue Glu166 mutated to glutamine (E166Q) acts as a loss-of function mutant in this assay (Figure 6A). To test whether the direct interaction with Plk4 is required for this function of FAM46C, we expressed in MM1.S cells the FAM46C(C320E/L321E) mutant, which reduces the binding with CBP1–2 of Plk4 (Figure 4B). Viability/proliferation of cells expressing FAM46C(C320E/L321E) was lower than the parental cells, but significantly higher than cells expressing the FAM46C(WT) (Figure 6A). We reasoned that the residual inhibitory effect of FAM46C(C320E/L321E) may be due to the fact that it maintains weak binding to Plk4 (Figure 4B). We therefore introduced the K144P/C320E/L321E triple mutations to FAM46C, which disrupt the FAM46C/CPB1–2 interaction more severely because both interfaces I and II are perturbed (Figure 4B). The results show that the triple mutations completely abolished the inhibitory effect of FAM46C on the cell viability/proliferation (Figure 6B).

We examined the enzymatic activity of the E158Q, C312E/L313E and K136P/C312E/L313E mutants of FAM46D, corresponding to E166Q, C320E/L321E and K144P/C320E/L313E of FAM46C, respectively. As expected, FAM46D(E158Q) showed no poly(A) polymerase activity (Figure S5A). FAM46D(C312E/L313E) is equally active as the FAM46D wild type (Figure S5A), consistent with the fact that these mutations are targeted to the area on the middle domain that is far away from the active site. FAM46D(K136P/C312E/L313E)

displayed approximately 2-fold reduction in activity (Figure S5B), which is probably due to perturbation of the RNA entry site of the NTase domain by the K136P mutation. Based on the high degree of sequence similarity between FAM46C and FAM46D (Figure S1), FAM46C(C320E/L321E) and FAM46C(K144P/C320E/L321E) are likely enzymatically active. Therefore, the reduced or lack of inhibitory effects of these mutants on cell proliferation is due at least in part to disruption of the interaction with Plk4. Taken together, our results suggest that the inhibition of cell viability/proliferation by FAM46C requires both its catalytic activity and the interaction with Plk4.

Discussion

Our crystal structure of FAM46C provides a basis for the poly(A) polymerase activity of the FAM46 family proteins. Mapping FAM46C mutations found in multiple myeloma to the crystal structure showed that most of the mutations likely cause either destabilization of the protein or disruption of the enzyme active site, consistent with the notion that FAM46C acts as a tumor suppressor. The direct interaction between FAM46 and Plk4 shown here identifies a previously unknown molecular pathway in which FAM46C functions. Our crystal structures show that the CPB1–2 of Plk4 can simultaneously bind both FAM46C and Cep152 or Cep192, providing a molecular basis for the recruitment of FAM46C to the centrosome and suggesting a role of FAM46C in centrosome regulation. Notably, centrosome abnormalities have been reported to be prevalent and correlated with poor prognosis in multiple myeloma (Chng et al., 2006; Dementyeva et al., 2010; Maxwell and Pilarski, 2005). Our findings suggest a potential role of FAM46C mutations in centrosome abnormalities in multiple myeloma. Moreover, the Plk4-mediated localization of FAM46C to the centrosome may be linked to the recently reported role of FAM46C in the spermatid manchette (Zheng et al., 2019). There is evidence suggesting that the manchette is nucleated by the centrosome (Lehti and Sironen, 2016). It is tempting to speculate that FAM46C recruited to the centrosome by Plk4 uses its enzymatic activity to regulate the structure and function of manchette, which is essential for the proper development of spermatids and therefore male fertility. The interaction with Plk4 appears to be a conserved feature of the FAM46 family proteins, and therefore may underlie the cellular functions of other FAM46 family members, which are poorly understood at present.

Previous studies have shown that FAM46C has cytotoxic activity towards multiple myeloma cells, which depends on its poly(A) polymerase activity (Mroczek et al., 2017; Zhang et al., 2017; Zhu et al., 2017). We further show that the interaction with Plk4 is also important for the cell growth inhibition function of FAM46C. Taken together, these observations indicate a model in which FAM46C regulates cell proliferation by adding poly(A) tails to RNAs in centrosomes (Figure 6C). The presence of RNA in centrosomes has been reported by many studies, although the identities and functions of RNA in centrosomes remain unclear (Alliegro et al., 2006; Chichinadze et al., 2013; Kingsley et al., 2007; Marshall and Rosenbaum, 2000). Functions hypothesized for RNA in centrosomes include mediating local protein translation and serving as scaffolds for the assembly of protein components in PCM (Alliegro, 2011; Chichinadze et al., 2013; Jao et al., 2017). One study has shown that CPEB and Maskin, two factors that control poly(A)-induced translation, are present in centrosomes and regulate local translation of the cell cycle regulator cyclin B1 (Groisman et al., 2000).

This study further showed that disruption of poly(A)-induced translation inhibits cell division and causes centrosome defects. FAM46C may regulate RNA stability and translation through polyadenylation in centrosomes. Future studies will address how this activity of FAM46C influences centrosome structure and function.

Star methods

RESOURCE AVAILABILITY

Lead contact.—Further information and requests for resources and reagents should be directed to and will be fulfilled by the Lead Contact, Xuewu Zhang (xuewu.zhang@utsouthwestern.edu).

Materials availability.—All the constructs generated in this study are available upon request.

Data and code availability.—The structure factors and atomic coordinates of FAM46C, the FAM46C/CPB1–2 complex, the FAM46C$^{E166Q/F193D/F206D}$/CPB1–2 complex, and the FAM46C/CPB1–2/CEP192 complex have been deposited to the protein data bank under the accession codes of 6W36, 6W38, 6W3I and 6W3J, respectively.

EXPERIMENTAL MODEL AND SUBJECT DETAILS

The study focused on the structure of human proteins, which was expressed in E. coli BL21(DE3). The peptide used in this study was synthesized chemically. HEK293T(female), U2OS (female), and MM1.S (female) cell lines were purchased from ATCC. Cell line identities were authenticated by the provider.

METHOD DETAILS

Cell and bacterial culture.—HEK293T (ATCC, #CRL-3216) and U2OS (ATCC, #HTB-96) cell were maintained in DMEM (ThermoFisher, #10566016) with 10% FBS (Thermo Fisher, #16000044) in a humidified tissue culture incubator supplemented with 5% CO_2. MM1.S cells were purchased from ATCC (CRL-2974) and cultured in RPMI1640 medium (ThermoFisher, #11875119) supplemented with 10% FBS in a humidified tissue culture incubator supplemented with 5% CO_2. The U2OS stable cell lines generated in this study were maintained in the DMEM medium with 10% tetracycline free FBS (GE Healthcare, #SH30070.03T). E. coli BL21(DE3) were cultured in LB medium at 37 °C with constant shaking at speed of 200 rpm. Protein expression was induced by adding 0.2 mM IPTG when the optical density (O.D.) of the culture reached 0.6 at 16 °C for 12 hours. For expression of seleno-methionine replaced protein, BL21(DE3) cells were cultured in M9 minimal medium until O.D. reached 0.6. The culture was supplemented with L-amino acids seleno-methionine (50 mg/L) (Sigma, #3211-76-5), lysine (100 mg/L), threonine (100 mg/L), phenylalanine (100 mg/L), leucine (50 mg/L), isoleucine (50 mg/L and valine (50 mg/L), and then induced with 0.2 mM IPTG at 16 °C for 12 hours.

Co-immunoprecipitation of FAM46C and Plk4.—Full-length human FAM46C with a Myc-tag and Plk4 with a FLAG-tag were cloned into the pRK5 vector (BD PharMingen,

#556104). HEK293T cells were transfected with the plasmids with Fugene HD (Promega, #E2311) according to the manufacturer's instruction. Cell were harvested 36 hours after transfection and lysed with a lysis buffer containing 50 mM Tris (pH 8.0), 150 mM NaCl, 0.1% NP-40, 1 mM DTT and protease inhibitor (Sigma, P8340). Lysates were centrifuged at 15000 rpm for 10 minutes at 4 °C, and the supernatant was transferred into a new tube. Anti-FLAG beads (Sigma, #A2220) were added into the supernatant, and the mixture were rotated at 4 °C for 1 hour. The beads were washed with the lysis buffer three times. Proteins remaining on the beads were resolved with 4–20% gradient SDS-PAGE (Bio-Rad, #4561096) and detected by western blot using anti-FLAG (Sigma, #F1804) and anti-Myc antibodies (Cell Signaling Technology, #2276).

Cell viability/proliferation assay.—Full length FLAG-tagged human FAM46C WT, E166Q, C320E/L321E and K144P/C320E/L321E were cloned into a modified FU-CRW vector (Cai et al., 2011). Lentiviruses were generated by transfecting the FAM46C plasmids and packing plasmids into HEK293T cells. Supernatants were collected and filtered with 0.45 um filter. Viruses were concentrated by centrifuging at 26000 rpm for 2 hours at 4 °C. MM1.S cells were infected by the viruses and expression of the FAM46C protein was confirmed with anti-FLAG western blot. Cell viability and proliferation were measured 6 days after viral infection by using an assay based on conversion of 3-(4,5-dimethylthiazol-2-yl)-2,5-diphenyltetrazolium bromide (MMT) (Abcam, #ab211091) according to the manufacturer's instruction. For each group, five measurements were taken to obtain the mean and standard deviation. Three biological repeats were carried out for each group.

Localization of FAM46C and centrosome counting.—For examining cellular localization of FAM46C, cells were seeded on cover glasses in 6-well plates and transfected with FLAG-tagged FAM46C, HA-tagged Plk4 (wild type or the I670P mutant) in pRK5 vector. Thirty-six hours after transfection, cells were fixed with 4% paraformaldehyde for 10 minutes, permeabilized with 0.2% Triton X-100 for 15 minutes and blocked with 5% bovine serum albumin at room temperature for 1 hour. Cells were incubated with anti-HA (Novus Biologicals, #NB600–361), anti-Myc (Cell Signaling Technology, #2276) and anti-γ–tubulin (Abcam, #ab11317) antibodies for detecting of FAM46C, Plk4 and γ–tubulin, respectively. Fluorescence-labeled secondary antibodies (Alexa Fluor 488, Cy3 and Alexa Fluor 647 respectively) were used for immuno-staining. Nuclei were stained with DAPI (4, 6-diamidino-2-phenylindole). Images were acquired using a *DeltaVision Core* microscope and processed with deconvolution and z-stack quick projection.

For counting centriole numbers, U2OS cells stably expressing both the centrosome marker centrin2-GFP and tetracycline-transactivator (rtTA) were transfected with the lentiviral vectors pTY-centrin2-GFP-IRES-Blasticidin and pPB-CAG-rtTA-IRES-Hygromycin (Addgene, #102423). These cells were used for inducible expression of Plk4 and FAM46C by using the lentiviral vectors pTetO-Myc-PlK4, pTetO-HA-FAM46C-P2A-Myc-Plk4 or pTetO-HA-FAM46C (E166Q)-P2A-Myc-Plk4. TetO (tetracycline operator) drives simultaneous expression of HA-FAM46C and Myc-Plk4 via the cleavage peptide sequences P2A and T2A (Zhang et al., 2013). Protein expression was induced by adding 0.5 μg/ml doxycycline (Sigma, #D9891) into the medium. Forty-eight hours later, cells were fixed with

4% paraformaldehyde. Plk4 and FAM46C were detected by anti-Myc and anti-HA immunostaining. Images of random areas of cells were taken by using a *DeltaVision Core* microscope. Co-localized puncta of Plk4, centrin2-GFP and FAM46C were counted as centrioles.

Protein expression and purification.—The coding region for human FAM46C (residues 16–358, excluding N- and C-terminal extensions that are non-conserved and predicted to be unstructured) was cloned into a modified pET28a vector that encodes a N-terminal His_6-SUMO-tag. Mutations for testing the CPB1–2 binding residues were introduced by PCR-based mutagenesis. The E166Q/F193D/F206D mutant of FAM46C (residues 16–350) was cloned into the same vector. Native protein was expressed BL21(DE3) in LB medium, whereas seleno-methionine replaced protein was expressed by using the protocol as in (Van Duyne et al., 1993). Culture conditions of both are described above in the “Cell and bacterial culture conditions”. The tag was removed by treating with the SUMO protease. GST-tagged FAM46C and FAM46D were constructed by inserting the coding region of FAM46C (residues 16–358) or FAM46D (residues 7–340) into the pGEX-6P-1 vector (GE Healthcare). The coding regions for CPB1–2 of human PLK4 (residues 580–810) and PB3 (residues 883–965) of PLK4 were cloned into a modified pET28a vector for recombinant expression. The proteins were expressed and purified with affinity chromatography followed by gel filtration chromatography. Buffers used for the purification of CPB1–2 contained 500 mM NaCl, because the protein tended to precipitate at lower concentrations of salt. All other buffers contained 150 mM NaCl.

In vitro pulldown assays.—GST-fused FAM46C and FAM46D were used for pulldown binding assays with CPB1–2 or PB3 of Plk4. Protein mixes in the pulldown buffer containing 10 mM Tris pH 8.0, 150 mM NaCl, 0.1% NP-40 and 1 mM DTT were incubated at room temperature for 10 minutes. Proteins were captured with glutathione beads (GE Healthcare, #17075601) pre-equilibrated with the same buffer. Beads were washed with the pulldown buffer three times to remove unbound proteins. Proteins bound to beads were resolved by SDS-PAGE gels and stained with Commassie blue R250.

Phospho-tag gel assay.—Phos-tag reagent was purchased from VWR (#AAL-107). 10% SDS-PAGE gels containing 2.5 μM Phos-tag and 500 μM $MnCl_2$ were made according to the manufacture’s instruction. Phosphorylation reactions were carried out in the reaction buffer containing 10 mM Tris pH 7.5, 5 mM ATP, 5 mM $MgCl_2$ and 150 mM NaCl. The Plk4 kinase domain (residues 1–277), MBP and FAM46D were added into the reaction buffer and incubated for different time periods. Reactions were stopped by adding the SDS loading buffer. Samples were resolved on 10% Phos-tag SDS-PAGE gel and stained with Commassie blue R250.

Poly(A) polymerase assay.—Florescein-labeled 15-mer poly(A) oligos were synthesized (Integrated DNA Technologies) and dissolved in DEPC-treated water (Thermo Fisher, #R0603). Poly(A) polymerization reactions contained the RNA oligo (2.5 μM), ATP (1 mM), $MgCl_2$ (1 mM), RNase inhibitor (Thermo Fisher, #AM2694) and FAM46D (2.5 μM) in the reaction buffer (25 mM Tris pH 7.0, 50 mM KCl, 0.02 mM EDTA, 0.2 mM DTT,

and 10% glycerol). In reactions with CBP1–2, the molar ratio between FAM46D and CBP1–2 was 1:1. Reactions were initiated by incubating the mixes at 30 °C and stopped by adding the gel loading buffer containing 8 M urea, 20 mM Tris pH 8.0, 1 mM EDTA and 1% bromophenol blue. RNA products were separated by 15% SDS-PAGE with 8 M urea. Gel images were taken with a GE ImageQuant LAS 4000 imager.

Crystallization and structure determination.—Initial crystallization screens of native FAM46C at 5 mg/ml were carried out in 96-well plates through sitting drop vapor diffusion. Optimized crystallization conditions for both native FAM46C and seleno-methionine replaced FAM46C at 5 mg/ml were 1 M $(NH_4)_2SO_4$, 0.1 M Bis-Tris pH 6.0 and 1% PEG3350. Crystals were cryo-protected in the crystallization buffer supplemented with 20–25% glycerol and flash cooled in liquid nitrogen for Diffraction data collection at the beamline 19ID at the advanced photon source (Argonne, IL). Data were processed with the HKL2000 software (Otwinowski and Minor, 1997). The structure was solved by seleno-methionine single-wavelength anomalous dispersion (SAD) using the Phenix package (Adams et al., 2010). The Autobuild module in Phenix was used to build the initial model into the SAD electron density map. Subsequent model building and refinement step were conducted in Coot and Phenix, respectively (Emsley et al., 2010). Statistics for data collection and refinement are summarized in Table 1.

FAM46C and CPB1–2 of Plk4 mixed at equimolar ratio in 10 mM Tris, pH8.0, 150 mM NaCl and 1 mM DTT precipitated heavily. The proteins resolubilized when pH was adjusted to above 9.0 with 1 M Tris, and spontaneously crystallized within a few hours at 20 °C. The FAM46C/CPB1–2/Cep192 triple complex was formed by including the known CPB1–2 binding region of Cep192 (residues 214–242, synthesized by GenScript) and crystallized using the same method. Crystals were cryo-protected with 25% glycerol and flashed cooled for data collection in the same procedure as described above. Despite the large size, these crystals did not diffract to high resolution. The datasets of the FAM46C/CPB1–2 and FAM46C/CPB1–2/Cep192 complexes reached resolution of 4.5 and 4.4 Å, respectively (Supplemental Table 1). The structures were solved by molecular replacement using Phaser with the structures of CPB1–2 (PDB ID: 4N7Z) and FAM46C described above as search models (Mccoy et al., 2007). Model building and refinement were carried out in a similar manner as described above. Due to the low resolution, the refinement was restrained by using the high-resolution structures of apo-FAM46C and CPB1–2 as reference models as implemented in Phenix.

To improve the resolution, we sought to crystallize the FAM46C/PB1–2 complex in a different crystal form by introducing mutations to FAM46C to disrupt the crystal packing interactions in the original crystal form. Residues at the surface of FAM46C (with the E166Q mutation that renders the protein catalytically dead) that are involved in crystal packing but not in the binding interface for PB1–2 were targeted. The E166Q/F193D/F206D mutant of FAM46C and CPB1–2 co-crystallized in 25% v/v Pentaerythritol ethoxylate (15/4 EO/OH), 0.05 M Ammonium sulfate, 0.05 M BIS-TRIS pH 6.0, with shape that is drastically different from the crystals of the wild-type FAM46C/PB1–2 complex. A dataset of a different space group was collected to resolution of 3.8 Å (Table 1). The structure was solved by molecular replacement as above and refined without using reference models. The

refined electron density map is of excellent quality, with most sidechains of the protein clearly identifiable (Figure 2S). The Cep192 peptide failed to co-crystallize with FAM46C$^{F193D/F206D}$ in this crystal form, due to the fact that crystal packing interactions partially occupies the binding site on CPB1–2 for Cep192.

QUANTIFICATION AND STATISTICAL ANALYSIS

Statistics of X-ray diffraction data collection and structure refinement are summarized in Table 1. Software used for crystallography include HKL2000, Phenix 1.16, Coot 0.8. P-values in Figure 6 were calculated by two-tailed Student's t-test using Prism 8. The sample sizes in Figures 5 and 6 are described in the figure legends.

Supplementary Material

Refer to Web version on PubMed Central for supplementary material.

Acknowledgements.

We thank Hongtao Yu for discussions and microscope usage, and the structural biology laboratory at University of Southwestern Medical Center (UTSW) for assistance on crystallization and data collection. This work is supported in part by grants from the National Institutes of Health (1R01CA220283) and the Welch foundation (I-1702) to X.Z. X.Z. is Virginia Murchison Linthicum Scholars in Medical Research at UTSW. Results shown in this report are derived from work performed at the Argonne National Laboratory, Structural Biology Center at APS. Argonne is operated by University of Chicago Argonne, LLC, for the U.S. Department of Energy, Office of Biological and Environmental Research under Contract DE-AC02-06CH11357.

References

Adams PD, Afonine PV, Bunkoczi G, Chen VB, Davis IW, Echols N, Headd JJ, Hung LW, Kapral GJ, Grosse-Kunstleve RW, et al. (2010). PHENIX: a comprehensive Python-based system for macromolecular structure solution. Acta crystallographica 66, 213–221.

Alliegro MC (2011). The centrosome and spindle as a ribonucleoprotein complex. Chromosome Res 19, 367–376. [PubMed: 21287260]

Alliegro MC, Alliegro MA, and Palazzo RE (2006). Centrosome-associated RNA in surf clam oocytes. Proc Natl Acad Sci U S A 103, 9034–9038. [PubMed: 16754862]

Arquint C, Gabryjonczyk AM, Imseng S, Bohm R, Sauer E, Hiller S, Nigg EA, and Maier T (2015). STIL binding to Polo-box 3 of PLK4 regulates centriole duplication. Elife 4, e07888.

Barbieri M, Manzoni M, Fabris S, Ciceri G, Todoerti K, Simeon V, Musto P, Cortelezzi A, Baldini L, Neri A, et al. (2016). Compendium of FAM46C gene mutations in plasma cell dyscrasias. British journal of haematology 174, 642–645. [PubMed: 26456599]

Barragan I, Borrego S, Abd El-Aziz MM, El-Ashry MF, Abu-Safieh L, Bhattacharya SS, and Antinolo G (2008). Genetic analysis of FAM46A in Spanish families with autosomal recessive retinitis pigmentosa: characterisation of novel VNTRs. Ann Hum Genet 72, 26–34. [PubMed: 17803723]

Bettencourt-Dias M, Rodrigues-Martins A, Carpenter L, Riparbelli M, Lehmann L, Gatt MK, Carmo N, Balloux F, Callaini G, and Glover DM (2005). SAK/PLK4 is required for centriole duplication and flagella development. Curr Biol 15, 2199–2207. [PubMed: 16326102]

Bolli N, Avet-Loiseau H, Wedge DC, Van Loo P, Alexandrov LB, Martincorena I, Dawson KJ, Iorio F, Nik-Zainal S, Bignell GR, et al. (2014). Heterogeneity of genomic evolution and mutational profiles in multiple myeloma. Nature communications 5, 2997.

Boyd KD, Ross FM, Walker BA, Wardell CP, Tapper WJ, Chiecchio L, Dagrada G, Konn ZJ, Gregory WM, Jackson GH, et al. (2011). Mapping of chromosome 1p deletions in myeloma identifies FAM46C at 1p12 and CDKN2C at 1p32.3 as being genes in regions associated with adverse survival. Clinical cancer research : an official journal of the American Association for Cancer Research 17, 7776–7784. [PubMed: 21994415]

Cai H, Babic I, Wei X, Huang J, and Witte ON (2011). Invasive prostate carcinoma driven by c-Src and androgen receptor synergy. Cancer research 71, 862–872. [PubMed: 21135112]

Chapman MA, Lawrence MS, Keats JJ, Cibulskis K, Sougnez C, Schinzel AC, Harview CL, Brunet JP, Ahmann GJ, Adli M, et al. (2011). Initial genome sequencing and analysis of multiple myeloma. Nature 471, 467–472. [PubMed: 21430775]

Chichinadze K, Lazarashvili A, and Tkemaladze J (2013). RNA in centrosomes: structure and possible functions. Protoplasma 250, 397–405. [PubMed: 22684578]

Chng WJ, Ahmann GJ, Henderson K, Santana-Davila R, Greipp PR, Gertz MA, Lacy MQ, Dispenzieri A, Kumar S, Rajkumar SV, et al. (2006). Clinical implication of centrosome amplification in plasma cell neoplasm. Blood 107, 3669–3675. [PubMed: 16373658]

Coelho PA, Bury L, Shahbazi MN, Liakath-Ali K, Tate PH, Wormald S, Hindley CJ, Huch M, Archer J, Skarnes WC, et al. (2015). Over-expression of Plk4 induces centrosome amplification, loss of primary cilia and associated tissue hyperplasia in the mouse. Open Biol 5.

Cunha-Ferreira I, Bento I, Pimenta-Marques A, Jana SC, Lince-Faria M, Duarte P, Borrego-Pinto J, Gilberto S, Amado T, Brito D, et al. (2013). Regulation of autophosphorylation controls PLK4 self-destruction and centriole number. Curr Biol 23, 2245–2254. [PubMed: 24184099]

Dementyeva E, Nemec P, Kryukov F, Muthu Raja KR, Smetana J, Zaoralova R, Greslikova H, Kupska R, Kuglik P, and Hajek R (2010). Centrosome amplification as a possible marker of mitotic disruptions and cellular carcinogenesis in multiple myeloma. Leuk Res 34, 1007–1011. [PubMed: 20096458]

Diener S, Bayer S, Sabrautzki S, Wieland T, Mentrup B, Przemeck GK, Rathkolb B, Graf E, Hans W, Fuchs H, et al. (2016). Exome sequencing identifies a nonsense mutation in Fam46a associated with bone abnormalities in a new mouse model for skeletal dysplasia. Mamm Genome 27, 111–121. [PubMed: 26803617]

Dull T, Zufferey R, Kelly M, Mandel RJ, Nguyen M, Trono D, and Naldini L (1998). A third-generation lentivirus vector with a conditional packaging system. J Virol 72, 8463–8471. [PubMed: 9765382]

Emsley P, Lohkamp B, Scott WG, and Cowtan K (2010). Features and development of Coot. Acta crystallographica 66, 486–501. [PubMed: 20383002]

Etokebe GE, Zienolddiny S, Kupanovac Z, Enersen M, Balen S, Flego V, Bulat-Kardum L, Radojcic-Badovinac A, Skaug V, Bakke P, et al. (2015). Association of the FAM46A gene VNTRs and BAG6 rs3117582 SNP with non small cell lung cancer (NSCLC) in Croatian and Norwegian populations. PLoS ONE 10, e0122651. [PubMed: 25884493]

Groisman I, Huang YS, Mendez R, Cao Q, Theurkauf W, and Richter JD (2000). CPEB, maskin, and cyclin B1 mRNA at the mitotic apparatus: implications for local translational control of cell division. Cell 103, 435–447. [PubMed: 11081630]

Habedanck R, Stierhof YD, Wilkinson CJ, and Nigg EA (2005). The Polo kinase Plk4 functions in centriole duplication. Nature cell biology 7, 1140–1146. [PubMed: 16244668]

Herrero AB, Quwaider D, Corchete LA, Mateos MV, Garcia-Sanz R, and Gutierrez NC (2020). FAM46C controls antibody production by the polyadenylation of immunoglobulin mRNAs and inhibits cell migration in multiple myeloma. J Cell Mol Med.

Holland AJ, Fachinetti D, Zhu Q, Bauer M, Verma IM, Nigg EA, and Cleveland DW (2012). The autoregulated instability of Polo-like kinase 4 limits centrosome duplication to once per cell cycle. Genes & development 26, 2684–2689. [PubMed: 23249732]

Holland AJ, Lan W, Niessen S, Hoover H, and Cleveland DW (2010). Polo-like kinase 4 kinase activity limits centrosome overduplication by autoregulating its own stability. J Cell Biol 188, 191–198. [PubMed: 20100909]

Holm L, Kaariainen S, Rosenstrom P, and Schenkel A (2008). Searching protein structure databases with DaliLite v.3. Bioinformatics 24, 2780–2781. [PubMed: 18818215]

Hu JL, Liang H, Zhang H, Yang MZ, Sun W, Zhang P, Luo L, Feng JX, Bai H, Liu F, et al. (2020). FAM46B is a prokaryotic-like cytoplasmic poly(A) polymerase essential in human embryonic stem cells. Nucleic Acids Res 48, 2733–2748. [PubMed: 32009146]

Jao LE, Akef A, and Wente SR (2017). A role for Gle1, a regulator of DEAD-box RNA helicases, at centrosomes and basal bodies. Mol Biol Cell 28, 120–127. [PubMed: 28035044]

Khoueiry R, Sohni A, Thienpont B, Luo X, Velde JV, Bartoccetti M, Boeckx B, Zwijsen A, Rao A, Lambrechts D, et al. (2017). Lineage-specific functions of TET1 in the postimplantation mouse embryo. Nat Genet 49, 1061–1072. [PubMed: 28504700]

Kim TS, Park JE, Shukla A, Choi S, Murugan RN, Lee JH, Ahn M, Rhee K, Bang JK, Kim BY, et al. (2013). Hierarchical recruitment of Plk4 and regulation of centriole biogenesis by two centrosomal scaffolds, Cep192 and Cep152. Proc Natl Acad Sci U S A 110, E4849–4857. [PubMed: 24277814]

Kingsley EP, Chan XY, Duan Y, and Lambert JD (2007). Widespread RNA segregation in a spiralian embryo. Evol Dev 9, 527–539. [PubMed: 17976050]

Klebba JE, Buster DW, McLamarrah TA, Rusan NM, and Rogers GC (2015). Autoinhibition and relief mechanism for Polo-like kinase 4. Proc Natl Acad Sci U S A 112, E657–666. [PubMed: 25646492]

Kuchta K, Knizewski L, Wyrwicz LS, Rychlewski L, and Ginalski K (2009). Comprehensive classification of nucleotidyltransferase fold proteins: identification of novel families and their representatives in human. Nucleic Acids Res 37, 7701–7714. [PubMed: 19833706]

Kuchta K, Muszewska A, Knizewski L, Steczkiewicz K, Wyrwicz LS, Pawlowski K, Rychlewski L, and Ginalski K (2016). FAM46 proteins are novel eukaryotic non-canonical poly(A) polymerases. Nucleic Acids Res 44, 3534–3548. [PubMed: 27060136]

Lehti MS, and Sironen A (2016). Formation and function of the manchette and flagellum during spermatogenesis. Reproduction 151, R43–54. [PubMed: 26792866]

Leung GC, Hudson JW, Kozarova A, Davidson A, Dennis JW, and Sicheri F (2002). The Sak polo-box comprises a structural domain sufficient for mitotic subcellular localization. Nature structural biology 9, 719–724. [PubMed: 12352953]

Levine MS, Bakker B, Boeckx B, Moyett J, Lu J, Vitre B, Spierings DC, Lansdorp PM, Cleveland DW, Lambrechts D, et al. (2017). Centrosome Amplification Is Sufficient to Promote Spontaneous Tumorigenesis in Mammals. Developmental cell 40, 313–322 e315. [PubMed: 28132847]

Lopes CA, Jana SC, Cunha-Ferreira I, Zitouni S, Bento I, Duarte P, Gilberto S, Freixo F, Guerrero A, Francia M, et al. (2015). PLK4 trans-Autoactivation Controls Centriole Biogenesis in Space. Developmental cell 35, 222–235. [PubMed: 26481051]

Marshall WF, and Rosenbaum JL (2000). Are there nucleic acids in the centrosome? Curr Top Dev Biol 49, 187–205. [PubMed: 11005019]

Martin G, and Keller W (2007). RNA-specific ribonucleotidyl transferases. Rna 13, 1834–1849. [PubMed: 17872511]

Mason JM, Lin DC, Wei X, Che Y, Yao Y, Kiarash R, Cescon DW, Fletcher GC, Awrey DE, Bray MR, et al. (2014). Functional characterization of CFI-400945, a Polo-like kinase 4 inhibitor, as a potential anticancer agent. Cancer Cell 26, 163–176. [PubMed: 25043604]

Maxwell CA, and Pilarski LM (2005). A potential role for centrosomal deregulation within IgH translocation-positive myeloma. Med Hypotheses 65, 915–921. [PubMed: 16023302]

Mccoy AJ, Grosse-Kunstleve RW, Adams PD, Winn MD, Storoni LC, and Read RJ (2007). Phaser crystallographic software. Journal of Applied Crystallography 40, 658–674. [PubMed: 19461840]

Moyer TC, Clutario KM, Lambrus BG, Daggubati V, and Holland AJ (2015). Binding of STIL to Plk4 activates kinase activity to promote centriole assembly. J Cell Biol 209, 863–878. [PubMed: 26101219]

Mroczek S, Chlebowska J, Kulinski TM, Gewartowska O, Gruchota J, Cysewski D, Liudkovska V, Borsuk E, Nowis D, and Dziembowski A (2017). The non-canonical poly(A) polymerase FAM46C acts as an onco-suppressor in multiple myeloma. Nature communications 8, 619.

Nakel K, Bonneau F, Eckmann CR, and Conti E (2015). Structural basis for the activation of the C. elegans noncanonical cytoplasmic poly(A)-polymerase GLD-2 by GLD-3. Proc Natl Acad Sci U S A 112, 8614–8619. [PubMed: 26124149]

Ohta M, Ashikawa T, Nozaki Y, Kozuka-Hata H, Goto H, Inagaki M, Oyama M, and Kitagawa D (2014). Direct interaction of Plk4 with STIL ensures formation of a single procentriole per parental centriole. Nature communications 5, 5267.

Otwinowski Z, and Minor W (1997). Processing of X-ray Diffraction Data Collected in Oscillation Mode. Methods in enzymology 276, 307–326.

Park SY, Park JE, Kim TS, Kim JH, Kwak MJ, Ku B, Tian L, Murugan RN, Ahn M, Komiya S, et al. (2014). Molecular basis for unidirectional scaffold switching of human Plk4 in centriole biogenesis. Nature structural & molecular biology 21, 696–703.

Rual JF, Venkatesan K, Hao T, Hirozane-Kishikawa T, Dricot A, Li N, Berriz GF, Gibbons FD, Dreze M, Ayivi-Guedehoussou N, et al. (2005). Towards a proteome-scale map of the human protein-protein interaction network. Nature 437, 1173–1178. [PubMed: 16189514]

Sercin O, Larsimont JC, Karambelas AE, Marthiens V, Moers V, Boeckx B, Le Mercier M, Lambrechts D, Basto R, and Blanpain C (2016). Transient PLK4 overexpression accelerates tumorigenesis in p53-deficient epidermis. Nature cell biology 18, 100–110. [PubMed: 26595384]

Shimanovskaya E, Viscardi V, Lesigang J, Lettman MM, Qiao R, Svergun DI, Round A, Oegema K, and Dong G (2014). Structure of the C. elegans ZYG-1 cryptic polo box suggests a conserved mechanism for centriolar docking of Plk4 kinases. Structure 22, 1090–1104. [PubMed: 24980795]

Sillibourne JE, Tack F, Vloemans N, Boeckx A, Thambirajah S, Bonnet P, Ramaekers FC, Bornens M, and Grand-Perret T (2010). Autophosphorylation of polo-like kinase 4 and its role in centriole duplication. Mol Biol Cell 21, 547–561. [PubMed: 20032307]

Slevin LK, Nye J, Pinkerton DC, Buster DW, Rogers GC, and Slep KC (2012). The structure of the plk4 cryptic polo box reveals two tandem polo boxes required for centriole duplication. Structure 20, 1905–1917. [PubMed: 23000383]

Stark C, Breitkreutz BJ, Reguly T, Boucher L, Breitkreutz A, and Tyers M (2006). BioGRID: a general repository for interaction datasets. Nucleic Acids Res 34, D535–539. [PubMed: 16381927]

Van Duyne GD, Standaert RF, Karplus PA, Schreiber SL, and Clardy J (1993). Atomic structures of the human immunophilin FKBP-12 complexes with FK506 and rapamycin. J Mol Biol 229, 105–124. [PubMed: 7678431]

Vitre B, Holland AJ, Kulukian A, Shoshani O, Hirai M, Wang Y, Maldonado M, Cho T, Boubaker J, Swing DA, et al. (2015). Chronic centrosome amplification without tumorigenesis. Proc Natl Acad Sci U S A 112, E6321–6330. [PubMed: 26578792]

Walker BA, Boyle EM, Wardell CP, Murison A, Begum DB, Dahir NM, Proszek PZ, Johnson DC, Kaiser MF, Melchor L, et al. (2015). Mutational Spectrum, Copy Number Changes, and Outcome: Results of a Sequencing Study of Patients With Newly Diagnosed Myeloma. J Clin Oncol 33, 3911–3920. [PubMed: 26282654]

Walker BA, Wardell CP, Melchor L, Hulkki S, Potter NE, Johnson DC, Fenwick K, Kozarewa I, Gonzalez D, Lord CJ, et al. (2012). Intraclonal heterogeneity and distinct molecular mechanisms characterize the development of t(4;14) and t(11;14) myeloma. Blood 120, 1077–1086. [PubMed: 22573403]

Wong YL, Anzola JV, Davis RL, Yoon M, Motamedi A, Kroll A, Seo CP, Hsia JE, Kim SK, Mitchell JW, et al. (2015). Cell biology. Reversible centriole depletion with an inhibitor of Polo-like kinase 4. Science 348, 1155–1160. [PubMed: 25931445]

Zhang QY, Yue XQ, Jiang YP, Han T, and Xin HL (2017). FAM46C is critical for the anti-proliferation and pro-apoptotic effects of norcantharidin in hepatocellular carcinoma cells. Scientific reports 7, 396. [PubMed: 28341836]

Zhang Y, Pak C, Han Y, Ahlenius H, Zhang Z, Chanda S, Marro S, Patzke C, Acuna C, Covy J, et al. (2013). Rapid single-step induction of functional neurons from human pluripotent stem cells. Neuron 78, 785–798. [PubMed: 23764284]

Zheng C, Ouyang YC, Jiang B, Lin X, Chen J, Dong MZ, Zhuang X, Yuan S, Sun QY, and Han C (2019). Non-canonical RNA polyadenylation polymerase FAM46C is essential for fastening sperm head and flagellum in micedagger. Biol Reprod 100, 1673–1685. [PubMed: 31087039]

Zhu YX, Shi C-X, Jedlowski P, Kortum KM, Bruins L, Ahmann J, Braggio E, Wang X, and Stewart AK (2015). Identification of FAM46C As a Multiple Myeloma Repressor. Blood 126, 836.

Zhu YX, Shi CX, Bruins LA, Jedlowski P, Wang X, Kortum KM, Luo M, Ahmann JM, Braggio E, and Stewart AK (2017). Loss of FAM46C Promotes Cell Survival in Myeloma. Cancer research 77, 4317–4327. [PubMed: 28619709]

Highlights:

- The FAM46 family proteins interact with Plk4
- The CPB1–2 domains of Plk4 bind FAM46
- Plk4 recruits FAM46C to the centrosome
- No mutual enzymatic regulation between FAM46 and Plk4

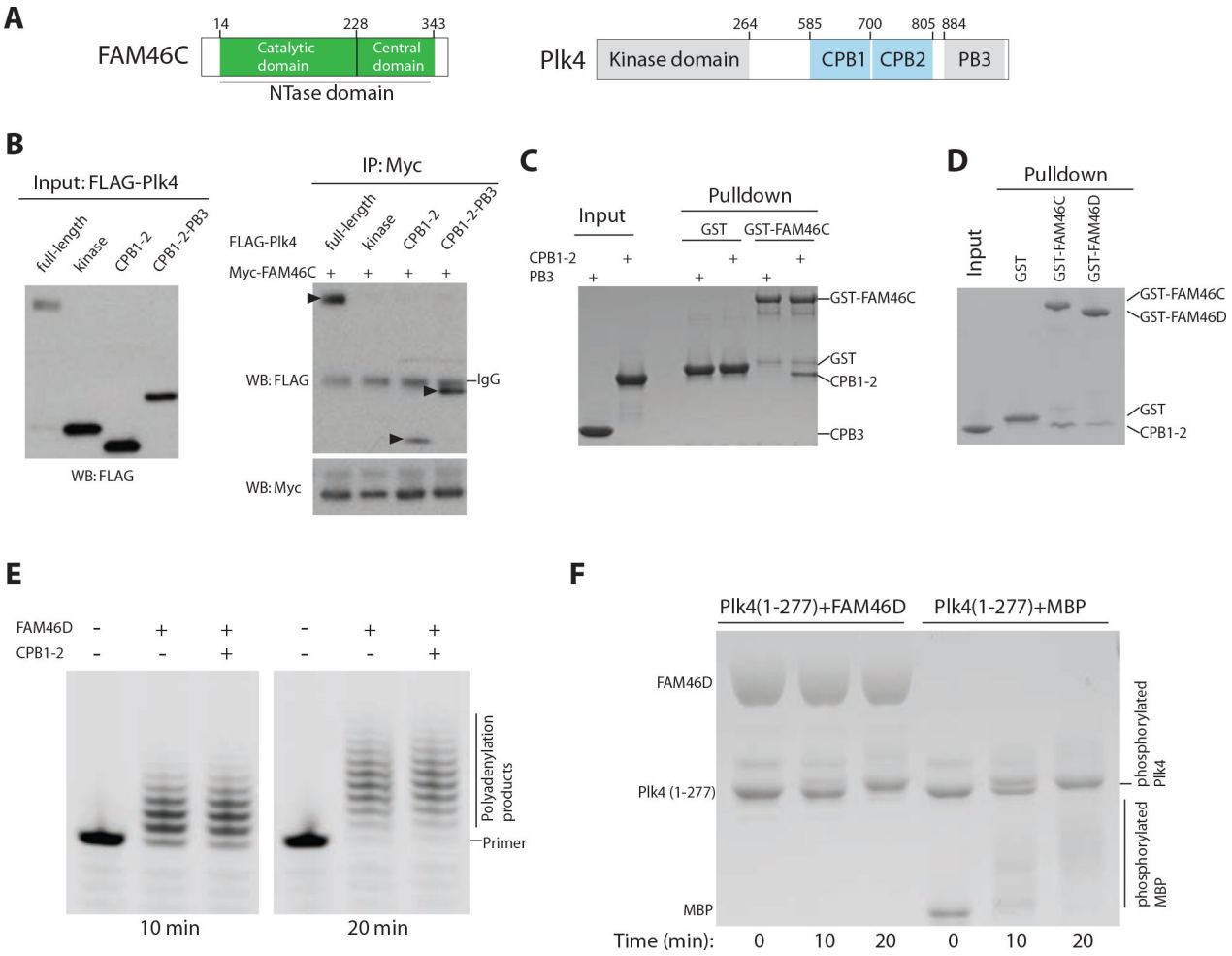

Figure 1. Direct interaction between FAM46 and CPB1–2 of Plk4.

(**A**) Domain structures of human FAM46C and Plk4. (**B**) Interaction between FAM46C and Plk4 in cells. Myc-tagged FAM46C and FLAG-tagged various constructs of Plk4 were co-transfected into HEK293T cells. Interactions were assessed by co-immunoprecipitation and western blot. Arrowheads indicate Plk4 domains pulled down by FAM46C. (**C**) FAM46C binds to CPB1–2 directly *in vitro*. GST-fused FAM46C pulled down CPB1–2, but not PB3, of Plk4. The GST protein was used as a negative control. (**D**) FAM46D binds to CPB1–2 of Plk4. (**E**) CPB1–2 does not affect the poly(A) polymerase activity of FAM46D. Reaction products with a Fluorescein-labelled $(A)_{15}$ oligo as the substrate were resolved on denaturing urea PAGE. (**F**) The NTase domain of FAM46D is not phosphorylated by Plk4. Products from phosphorylation reactions were resolved on a Phos-tag gel, where band shits indicate phosphorylation. Myelin basic protein (MBP) was used as the positive control. Substantial band shifts of both the kinase domain of Plk4 and MBP indicate robust phosphorylation. There was no shift of the FAM46D band.

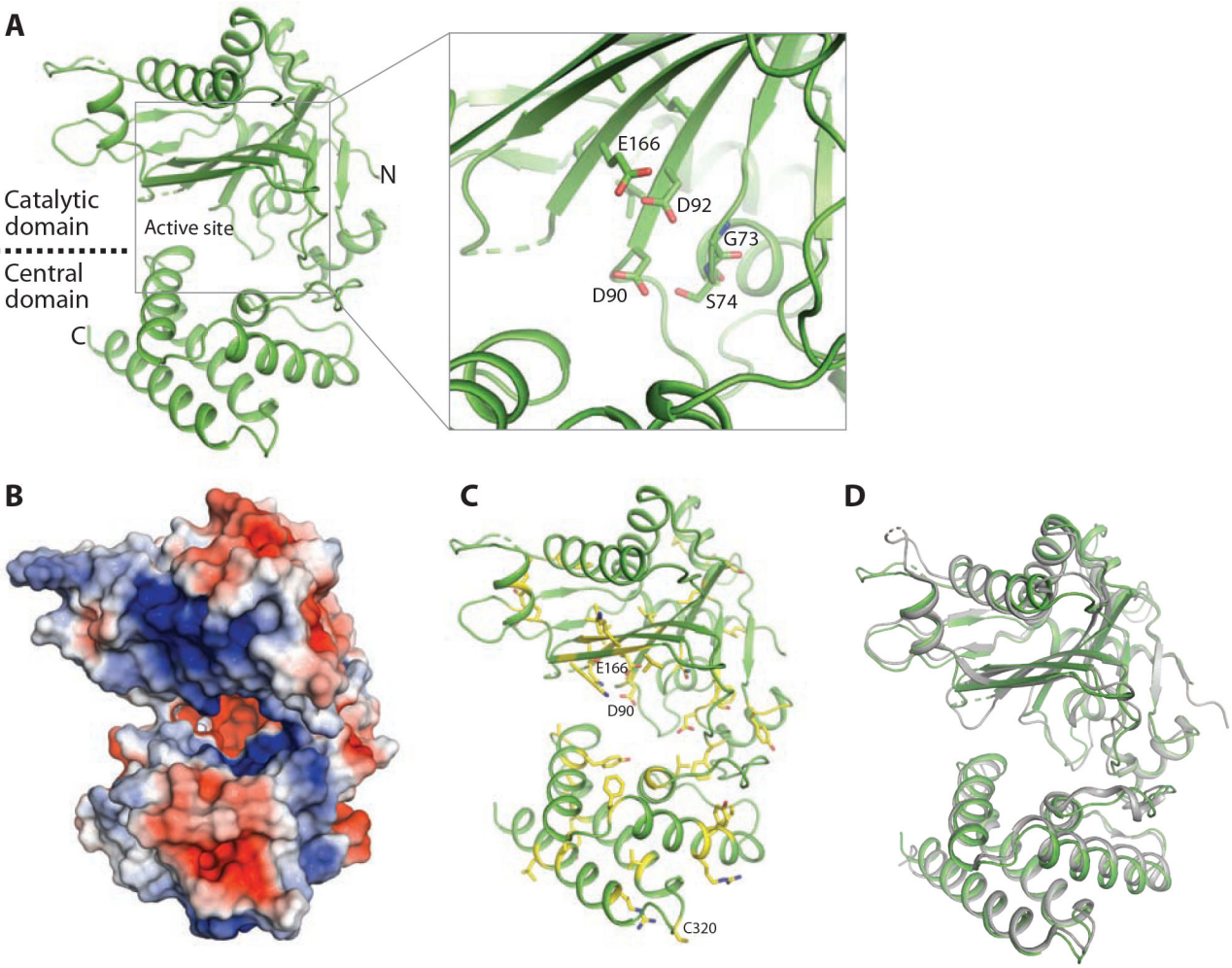

Figure 2. Crystal structure of human FAM46C.

(**A**) Overall structure of the NTase domain of FAM46C and detailed view of the active site residues. (**B**) Surface electrostatic potential of FAM46C. The red-to-blue color spectrum represents the range of electrostatic potential from −3 to 3 KT/e. (**C**) Mapping of FAM46C mutations found in multiple myeloma to the structure. The mutated residues are highlighted in yellow with sidechains shown. (**D**) Structure comparison of human FAM46C (green) and FAM46B from *Xenopus tropicalis* (gray; PDB ID: 6JYJ).

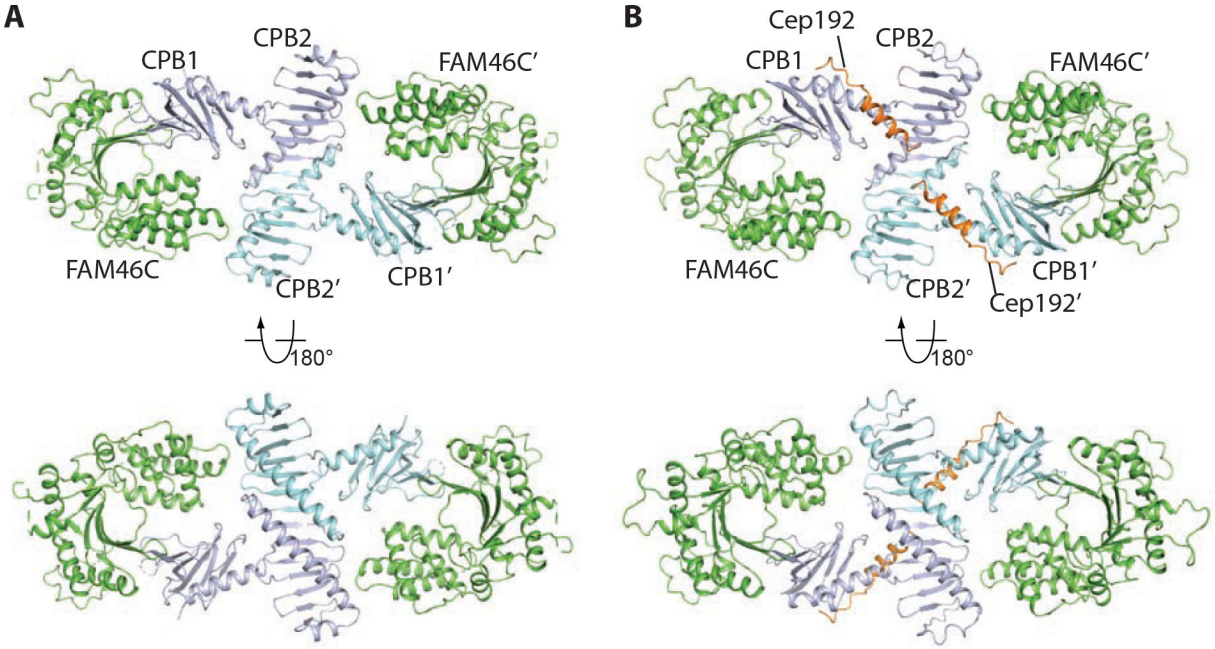

Figure 3. Crystal structure of the FAM46C/CPB1–2 and FAM46C/CPB1–2/Cep192 complexes.

(**A**) Two orthogonal views of the structure of the FAM46C/CPB1–2 complex. **(B)** Two orthogonal views of the structure of the FAM46C/CPB1–2/Cep192 complex.

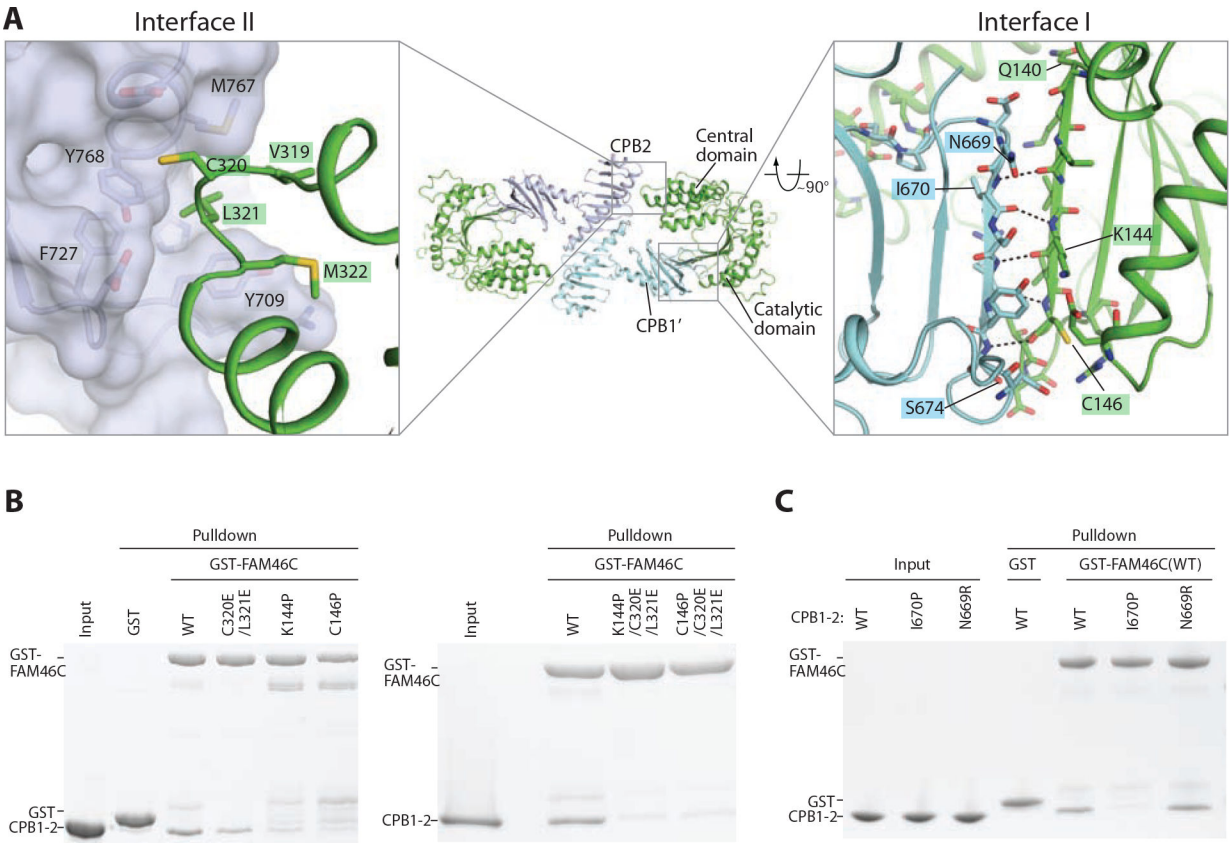

Figure 4. Binding interfaces between FAM46C and CPB1–2.

(**A**) Overview of the binding mode and detailed views of interfaces I and II between FAM46C and CPB1–2. (**B**) GST-pulldown assays showing that mutations of interface residues in FAM46C impair the FAM46C/CPB1–2 interaction. (**C**) GST-pulldown assays showing that mutations of interface residues in CPB1–2 impair the FAM46C/CPB1–2 interaction.

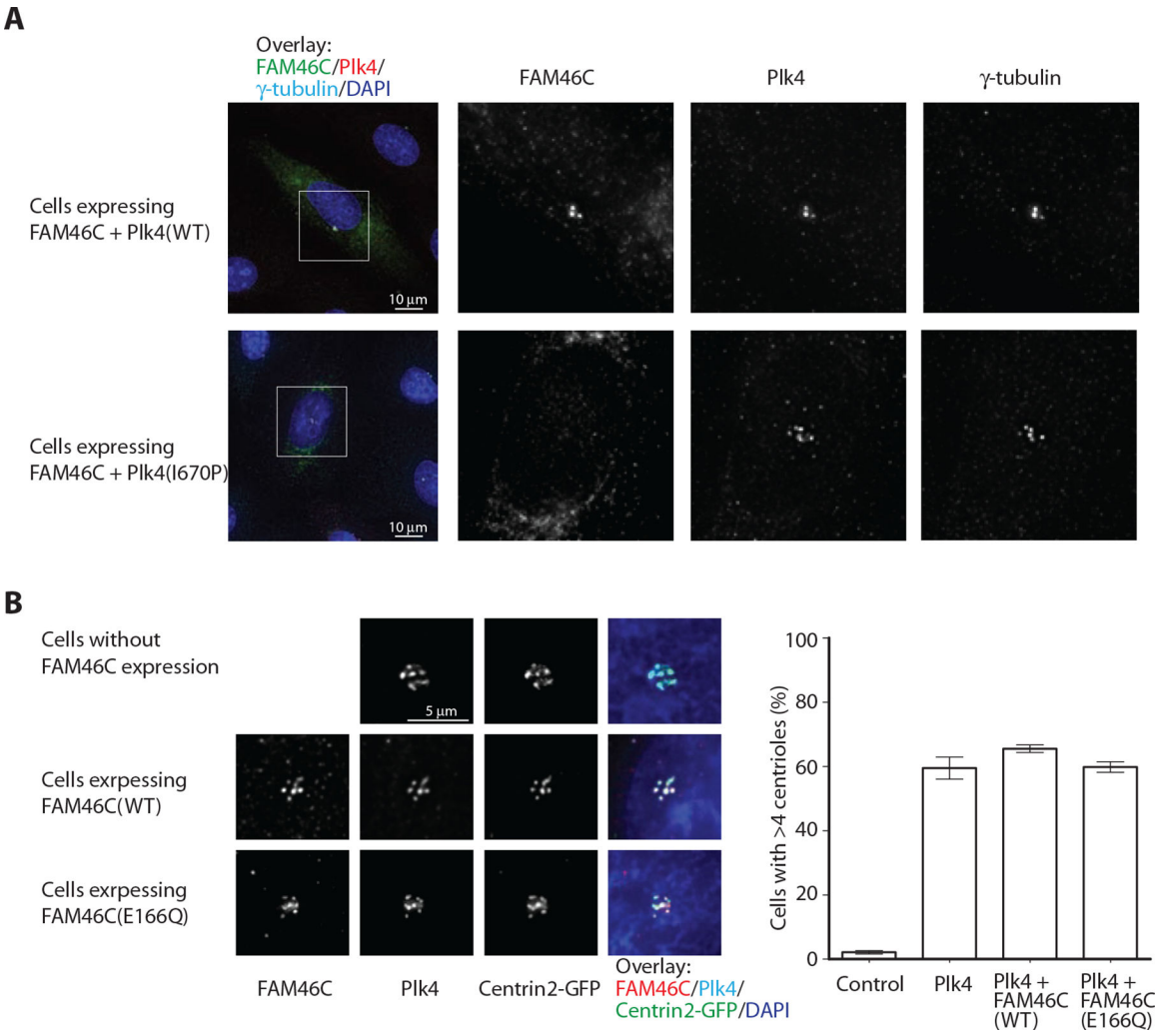

Figure 5. Recruitment of FAM46C by Plk4 to centrosomes.

(**A**) FAM46C is recruited to centrosomes by Plk4 WT, but not the I670P mutant. U2OS cells expressing FLAG-tagged FAM46C and HA-tagged Plk4 were immuno-stained for FAM46C, Plk4, -tubulin and nucleus. The three right panels show expanded views of the individual channels of the boxed region in the merged images on the left. (**B**) FAM46C does not affect Plk4-mediated centrosome overduplication. U2OS cells expressing various combinations of FAM46C and Plk4 were immuno-stained for counting centrosomes. Representative images of expanded views of centriole clusters are shown on the left. The bars and error bars on the right panel represent means and standard deviations, respectively. The experiments were repeated 3 times and more than 80 cells were counted for each group.

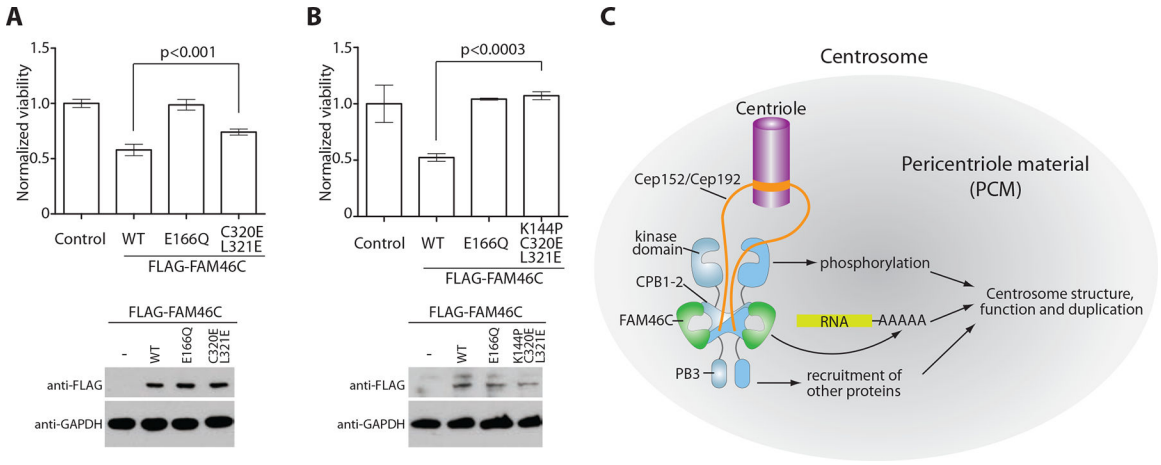

Figure 6. Inhibition of cell viability/proliferation by FAM46C is dependent on its interaction with Plk4.

(**A**) Viability assays of MM1.S cells expressing FAM46C WT, E166Q or C320E/L321E. The results were normalized against parental MM1.S cells that are not transfected with FAM46C constructs. For each group, cells from 5 wells were measured. The bars and error bars are means and standard deviations, respectively. The results shown are from one set out of three biological repeats. P-values were calculated by two-tailed Student's t-test. The lower panel shows that the express levels of the different FAM46C constructs were similar. (**B**) Viability assays of MM1.S cells expressing FAM46C WT, E166Q or K144P/C320E/L321E. The data are presented in the same manner as in (**A**). (**C**) Model of FAM46C recruitment to and function in centrosomes.

Table 1.

Diffraction data and structure refinement statistics.

	FAM46C-Native	FAM46C-SeMet	FAM46C/PLK4 complex	FAM46C/PLK4/CEP192 complex	FAM46C(Mutant)/PLK4 complex
Data collection					
Space group	$P2_12_12_1$	$P2_12_12_1$	I222	I222	$P3_121$
Cell dimensions					
a, b, c (Å)	51.7, 60.0, 173.0	52.0, 59.1, 173.7	87.4, 158.6, 165.5	88.0, 161.4, 167.5	142.3, 142.3, 147.9
α, β, γ (°)	90.00, 90.00, 90.00	90.00, 90.00, 90.00	90.00, 90.00, 90.00	90.00, 90.00, 90.00	90.00, 90.00, 120.00
Resolution (Å)	50.0–2.85(2.90–2.85)	50.0–2.90(2.95–2.90)*	50.0–4.50(4.58–4.50)	50.0–4.4(4.48–4.4)	50–3.8(3.87–3.80)
R_{sym} (%)	5.4(92.5)	7.6(80.1)	5.9(46.0)	9.9(77.5)	10.3(>100)
R_{pim}(%)	2.3(38.8)	2.2(24.6)	2.5(22.9)	2.3(20.0)	2.9(57.1)
I/σ	39.4(1.6)	29.9(2.7)	22.2(2.5)	26.9(2.1)	27.8(1.4)
$CC_{1/2}$#	0.849	0.958	0.847	0.891	0.892
Completeness (%)	99.2(95.0)	77.0(95.5)	94.0(74.2)	99.1(97.1)	100.0(100.0)
Redundancy	6.8(6.0)	12.6(10.9)	6.2(4.3)	18.7(13.3)	17.8(15.6)
Refinement					
Resolution (Å)	35.45–2.85(2.96–2.85)		46.7–4.5(4.65–4.49)	37.2–4.4(4.54–4.38)	47.3–3.8(3.94–3.80)
No. reflections	12754		6111	6730	14345
R_{work}/R_{free} (%)	21.5(35.4)/25.9(44.6)		23.2(22.9)/29.6(37.1)	26.3(27.6)/31.4(34.8)	21.7(29.0)/26.1(34.7)
No. atoms					
Protein	2632		4423	4608	4342
Ligand/ion	15		0	0	0
Water	0		0	0	0
B-factors					
Protein	123.66		88.11	67.58	55.94
Ligand/ion	209.80				
Water					
R.m.s deviations					
Bond lengths (Å)	0.002		0.004	0.004	0.004
Bond angles (°)	0.474		1.18	1.07	0.729
Ramanchandran plot					
Favored (%)	92.79		92.05	91.09	91.46
Allowed (%)	6.9		6.65	7.66	7.78
Disallowed (%)	0.31		1.29	1.25	0.76

*Numbers in parenthesis are for the highest resolution shell.

#$CC_{1/2}$ values shown are for the highest resolution shell.

KEY RESOURCES TABLE

REAGENT or RESOURCE	SOURCE	IDENTIFIER
Antibodies		
Chicken polyclonal anti-HA	Novus Biologicals	Cat# NB600-361
Mouse monoclonal anti-Myc	Cell Signaling Technology	Cat# 2276
Mouse monoclonal anti-FLAG	Sigma	Cat# F1804
Rabbit polyclonal anti-γ-tubulin	Abcam	Cat# ab11317
Goat anti-Mouse IgG, Alexa Fluor 488	Thermo Fisher	Cat# A32723
Goat anti-Rabbit IgG, Cyanine3	Thermo Fisher	Cat# A10520
Goat anti-Chicken IgY, Alexa Fluor 647	Thermo Fisher	Cat# A21449
Bacterial and Virus Strains		
BL21 (DE3)	New England Biolabs	Cat# C2527I
Lentivirus	Dull et al., 1998	N/A
Biological Samples		
Fetal Bovine Serum, Tetracycline free	GE Healthcare	Cat# SH30070.03T
Fetal Bovine Serum	Thermo Fisher	Cat# 16000044
Chemicals, Peptides, and Recombinant Proteins		
Cep192 peptide (214–242)	GenScript	N/A
Fluorescein-labeled 15-mer poly(A)	Integrated DNA Technologies	N/A
RNase inhibitor	Thermo Fisher Scientific	Cat# AM2694
Phos-tag	VWR	Cat# AAL-107
Fugene HD	Promega	Cat# E2311
protease inhibitor	Sigma	Cat# P8340
Anti-FLAG beads	Sigma	Cat# A2220
4–20% gradient SDS-PAGE	Bio-Rad	Cat# 4561096
glutathione beads	GE Healthcare	Cat# 17075601
DMEM	Thermo Fisher	Cat# 10566016
RPMI1640	Thermo Fisher	Cat# 11875119
doxycycline	Sigma	Cat# D9891
Seleno-methionine	Sigma	Cat#3211-76-5
DEPC-treated water	Thermo Fisher	Cat# R0603
Critical Commercial Assays		
MMT assay kit	Abcam	Cat# ab211091
Deposited Data		
FAM46C	This study	6W36
FAM46C/CPB1–2	This study	6W38
FAM46CE166Q/F193D/F206D/CPB1–2	This study	6W3I
FAM46C/CPB1–2/CEP192	This study	6W3J
CPB1–2/Cep192	Park et al., 2014	4N7Z

REAGENT or RESOURCE	SOURCE	IDENTIFIER
CPB1–2	Park et al., 2014	4N9J
FAM46B	Hu et al., 2020	6JYJ
Experimental Models: Cell Lines		
HEK293T	ATCC	Cat# CRL-3216
U2OS	ATCC	Cat# HTB-96
MM1.S	ATCC	Cat# CRL-2974
Oligonucleotides		
All oligonucleotides are listed in Table S1	This study	N/A
Recombinant DNA		
pPB-CAG-rtTA-IRES-Hygromycin	Khoueiry et al., 2017	RRID: Addgene_102423
Human Plk4 cDNA	Horizon Discovery	Cat# MHS6278-202808533
Human FAM46C cDNA	Horizon Discovery	Cat# MHS6278-202808213
pRK5	BD PharMingen	Cat# 556104
pGEX6P1	GE Healthcare	Cat# 28954648
pET28a	Novagen	Cat# 69864
FU-CRW	Cai et al., 2011	N/A
pTY-centrin2-GFP-IRES-Blasticidin	This study	N/A
pTetO-Myc-PlK4	This study	N/A
pTetO-HA-FAM46C-P2A-Myc-Plk4	This study	N/A
pTetO-HA-FAM46C (E166Q)-P2A-Myc-Plk4	This study	N/A
Software and Algorithms		
HKL2000	Otwinowski et al, 1997	https://hkl-xray.com
Phenix	Adams et al, 2010	http://www.phenix-online.org
Coot	Emsley et al, 2010	https://www2.mrc-lmb.cam.ac.uk/personal/pemsley/coot/
Prism	GraphPad Software	https://www.graphpad.com/guides/prism/7/curve-fitting/index.htm
Pymol	Schrodinger, LLC	https://pymol.org/2/
Phaser	Mccoy et al, 2007	http://www.ccp4.ac.uk/html/phaser.html